Coupled Inductor Characterization for a High Performance Interleaved Boost Converter

Hiroyuki Kosai[1], Seana McNeal[2], Brett Jordan[2], James Scofield[2], Biswajit Ray[3], and Zafer Turgut[1]

[1]UES, Inc., Dayton, OH 45432 USA
[2]Air Force Research Laboratory, Wright Patterson Air Force Base, WPAFB, OH 45433 USA
[3]Bloomsburg University of Pennsylvania, Bloomsburg, PA 17815 USA

Interleaved power converter topologies have received increasing attention in recent years for high power and high performance applications. The advantages of interleaved boost converters include increased efficiency, reduced size, reduced electromagnetic emission, faster transient response, and improved reliability. The front end inductors in an interleaved boost converter are magnetically coupled to improve electrical performance and reduce size and weight. Compared to a direct coupled configuration, inverse coupling provides the advantages of lower inductor ripple current and negligible dc flux levels in the core. In this paper, we explore the possible advantages of core geometry on core losses and converter efficiency. Analysis of FEA simulation and empirical characterization data indicates a potential superiority of a square core, with symmetric 45° energy storage corner gaps, for providing both ac flux balance and maximum dc flux cancellation when wound in an inverse coupled configuration.

Index Terms—**Interleaved boost converter, magnetic core, magnetic flux.**

I. Introduction

INTERLEAVED buck and boost converters have been studied in recent years to improve power converter performance in terms of efficiency, size, conducted electromagnetic emission, and transient response. The benefits of interleaving include high power capability, modularity, and improved reliability. However, an interleaved topology improves converter performance at the cost of additional inductors, power switching devices, and output rectifiers. Since the inductor is the largest and heaviest component in a power boost converter, the use of a coupled inductor instead of multiple discrete inductors is preferred. Coupled inductors also offer additional advantages such as reduced core and winding loss as well as improved input and inductor current ripple [1]–[3].

Performance improvements of two-phase interleaved boost converters (IBCs) using an E-E core coupled inductor have been reported in [1]–[5], and optimization of E-I core-based coupled inductors for an IBC was presented in [6] and [7].

The focus of the present paper is to optimize the coupled inductor design in relation to maximizing the dc flux cancellation, an important criterion for high power converters. To achieve this goal, an experimental investigation was carried out to study the dc field cancellation effects of various core configurations for the coupled inductor including: E-E core, square core with 90° gap, and square core with 45° gap. The data conclusively identified the square core with 45° gap as providing the best mix of ac flux balance and dc flux cancellation. This conclusion was verified experimentally by comparison in a 2-kW dc-dc IBC operating at a switch frequency of 78 kHz. The following section briefly summarizes key IBC performance analysis considerations, while subsequent sections describe experimental and simulated inductor performance parameters for the three designs.

Manuscript received March 07, 2009. Current version published September 18, 2009. Corresponding author: H. Kosai (e-mail: hiroyuki.kosai@wpafb.af.mil).

Color versions of one or more of the figures in this paper are available online at http://ieeexplore.ieee.org.

Digital Object Identifier 10.1109/TMAG.2009.2024639

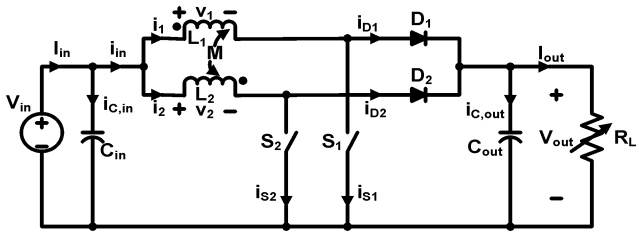

Fig. 1. Circuit schematic of an interleaved boost dc-dc converter.

II. DC/DC Converter Performance Analysis

The schematic of an inverse-coupled IBC is shown in Fig. 1. Detailed derivations for inductor currents and equivalent inductances for an IBC under continuous inductor current mode (CICM) operation are presented in [1]. These derivations are used to study the effect of inductor coupling on the converter's inductor and input ripple currents, minimum load current requirement for CICM operation, and flux levels in the coupled inductor core.

Summarizing, a coupled inductor with a mutual inductance, M, and equal self inductances, L, yield a coupling factor $k = M/L$, from which the basic voltage and current relationships for a coupled inductor are given by the following:

$$v_1 = L\frac{di_1}{dt} - M\frac{di_2}{dt} \tag{1}$$

$$v_2 = L\frac{di_2}{dt} - M\frac{di_1}{dt}. \tag{2}$$

Applying volt-sec balance to either winding of the coupled inductor yields the dc voltage gain equation, $V_{\rm out}/V_{\rm in} = 1/(1-D)$, consistent with conventional CICM boost converter theory.

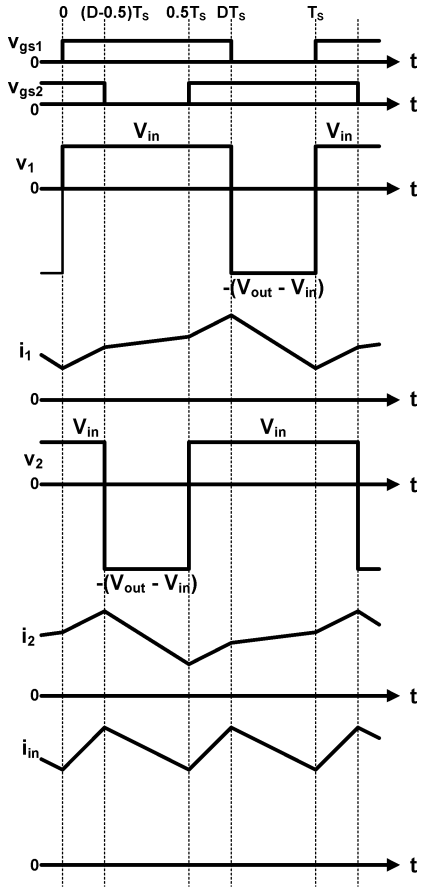

Fig. 2. Theoretical waveforms of an inverse coupled boost converter.

Fig. 2 illustrates the resulting theoretical voltage and current waveforms of an inverse coupled IBC.

Calculations for magnetic flux density and associated currents that generate the flux are accomplished using a transformer-like equivalent circuit for the coupled inductor. Accordingly, (1) and (2) are rearranged to derive explicit expressions for voltage across the mutual and leakage inductances. Expressions for the fluxes (ϕ_1 and ϕ_2) crossing each winding are also derived [1] using the following:

$$v_1 = N\frac{d\phi_1}{dt} = (L-M)\frac{di_1}{dt} + M\frac{d(i_1-i_2)}{dt} \tag{3}$$

$$v_2 = N\frac{d\phi_2}{dt} = (L-M)\frac{di_2}{dt} - M\frac{d(i_1-i_2)}{dt} \tag{4}$$

$$v_M = M\left(\frac{di_1}{dt} - \frac{di_2}{dt}\right). \tag{5}$$

For CICM operation, voltages across the windings are identical throughout the period; therefore, the total ac flux across each winding is equal. AC voltages across the windings are the sum of the voltage across M and the voltage across L. Since induced voltage is related to flux by Faraday's law, the mutual and leakage fluxes can therefore be determined.

The main source of flux leakage is introduced by core gaps. Outside these windings, flux associated with leakage takes a shorter path (i.e., through the air) and is uncoupled. Flux associated with mutual inductance travels through both set of windings, a large portion of which remains in the core. It can be shown that for a given input voltage, the mutual flux density is independent of duty ratio for inverse-coupled configuration, and it is duty ratio dependent for direct-coupled configuration. From this, it follows that the mutual flux density ratio between inverse and direct-coupled configurations is 1/(2D-1). Accordingly, the mutual flux induced core losses would be significantly higher in the inverse-coupled configuration, especially for D approaching 0.5. It should be noted that ac flux in the core is not related to an IBC's dc output current.

In the dc environment where two windings share the dc current equally, the inverse-coupled configuration cancels most flux in the core since the flux generated by the two windings has opposing polarity. At the core directly underneath the windings of N turns each, the resultant flux is $(1-k)LI_{\rm dc}/N$, where $I_{\rm dc}$ is dc current through the winding. For the direct-coupled configuration, the flux generated by two windings will add rather than cancel within the core, which is $(1+k)LI_{\rm dc}/N$. As a result, direct-coupling configurations will saturate the core more readily when operated at a high output current. The dc flux consideration represents a significant benefit to using inverse-coupled configuration in high power dc applications. Conversely, ac flux is minimized in direct coupling mode.

TABLE I
INDUCTOR PARAMETERS

Inductor type	# of turns per leg	Air gap (mm)	L (μH)	M (μH)	k	μ_r
E-E core	14	3.4	33.6	23.1	0.69	1680
Square 90° gap	20	1.6	35.9	25.4	0.71	500
Square 45° gap	16	2.8	32.4	20.1	0.64	2500

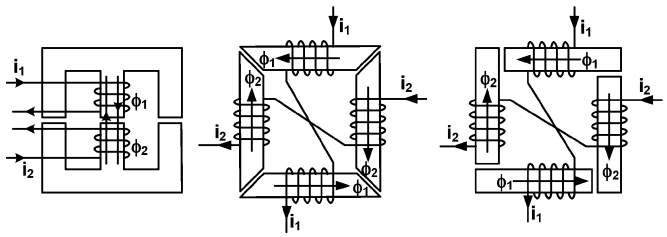

Fig. 3. Winding configuration of the coupled inductors (L to R: E-E core, square 45° gap core, and square 90° gap core).

III. MAGNETIC FIELD AND DC FLUX CANCELLATION ANALYSIS AND SIMULATION

Table I lists design parameters for the three coupled inductors evaluated for this paper in which the gaps were adjusted to generate a similar k and windings were scaled so that the inductances closely matched. Fig. 3 shows their configurations.

Using these parameters, models were created in QuickField 5.6 Professional Version, and used to perform two groups of simulations. One ampere-turn winding excitation was used for all computations of dc flux distributions in the inverse coupled

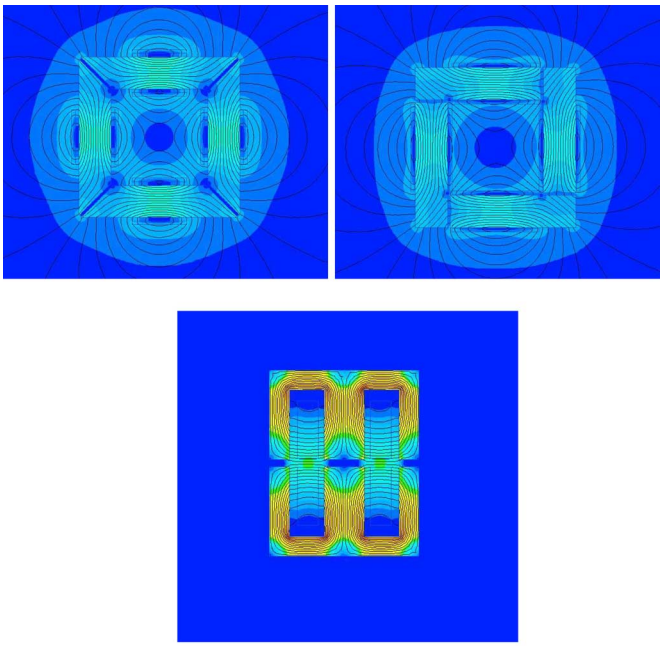

Fig. 4. Flux density map for normalized inductor models (CW from top left: square 45° gap core, square 90° gap core, E-E core, and legend).

inductor models. The first simulations used physical models that reflected the tested inductors' actual geometries and permeabilities.

The second simulation group consisted of modifying the physical models to equalize cross sectional areas, permeabilities, gap length, and magnetic flux path lengths of the E-E and 45° gap core inductors to that of the square 90° gap core inductor model. Since there are four gaps for both the 45° and the 90° core inductor, the two outer leg gaps of the E-E core were set to twice the gap dimension of the other two inductors. Fig. 4 shows the simulated dc flux density characteristics of the three coupled inductor models during inversely coupled operation with one ampere-turn input. As can be seen in Fig. 4, the E-E core produced the highest peak and average value of flux density of the three cores considered. While only a 0.2-G difference was predicted between the peak flux values of the two square cores, the 90° gap core had the lower predicted flux density. From these simulations, verification of significant dc flux cancellation in inverse coupled configurations is confirmed, as is the apparent superiority of square geometries.

These results confirm the predicted suitability of the inverse coupled winding configuration for high power IBCs. In addition, these results illustrate the potential benefit that coupled inductor IBCs offer in terms of reduced magnetic component volume and weight.

IV. Experimental Results

A power IBC was prototyped and tested to experimentally characterize the three coupled inductor designs and compare

TABLE II
Boost Converter Efficiency Data

Inductor type	V_{in} (V)	I_{in} (A)	V_{out} (V)	I_{out} (A)	P_{out} (W)	Converter efficiency (%)
E-E core	60.0	27.57	158.7	9.69	1538	93.0
Square 90° gap	60.0	27.44	158.8	9.64	1531	93.0
Square 45° gap	60.0	27.20	158.8	9.79	1555	95.2

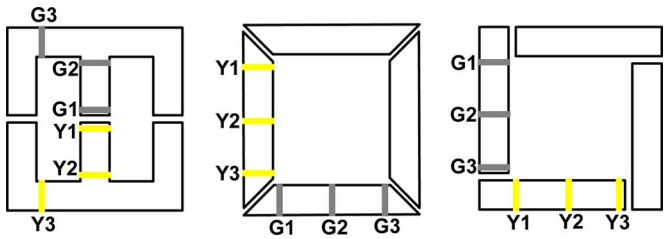

Fig. 5. Pickup coil location for the coupled inductors.

to simulation results. Each leg of the 100 V/270 V, 2-kW power stage consists of four MOSFETs (IRFP27N60) and four Schottky diodes (CSD20030D). The output filter capacitance consists of two 30 μF X7R ceramic capacitors. Each leg of the converter was switched at a frequency of 78 kHz with a phase shift of 180° between the two sides. Inductor current sharing between legs was found to be within $\pm 5\%$ for all three inductors, indicating good balance between winding pairs and core gaps. It was also observed that converter waveforms are effectively independent of inductor design, reflective of the good L, M and thus impedance correspondence between the different geometries. Table II shows the associated 1.5-kW converter efficiency data collected from the prototype IBC operating with each of the three inductors. The apparent 2% efficiency advantage of the 45° gap square core, seen in Table II, was determined to be due primarily to the use of a low-loss ferrite (P material from Magnetics, Inc.).

To study the flux leakage and dc flux cancellation process as well as measuring the ac flux density in the magnetic core, several one-turn pickup coils were placed at the center and adjacent to two core windings, as shown in Fig. 5.

For this study, a function generator was used to apply a 4-V, 78-kHz sine wave signal across only one winding coil on which Y1, Y2, and Y3 pickup coils were placed. Using the induced voltages at all six pickup coils, the input voltage, and current to the winding, induced fluxes crossing through the pickup coils for 1 A of input current were calculated as shown in Table III. Except for the E-E core inductor, the experimental results were in reasonable agreement with simulated results. Possible reasons for the discrepancies between experimental and simulated values are gap distance measurement errors and the fact that QuickField is a 2-D simulation tool rather than 3-D.

From this table, the field distributions for the square 45° gap core inductor were found to be more uniform throughout the core than the other inductor types. This means that the ratio of flux leakages at the gaps with respect to the total flux leakages is greatest for the square 45° gap core inductor. Since the

TABLE III
CALCULATED AND SIMULATED AC FLUX FOR 1 A THROUGH THE COIL ON WHICH Y1, Y2, AND Y3 PICKUP COILS ARE PLACED

Inductor type	Y1 (μWb)	Y2 (μWb)	Y3 (μWb)	G1 (μWb)	G2 (μWb)	G3 (μWb)
E-E core	1.76	2.07	0.84	1.45	1.58	0.69
Simulation (E-E)	1.36	1.85	0.90	1.24	1.32	0.64
Square 45° gap	1.65	1.96	1.67	1.30	1.42	1.28
Simulation (45° gap)	1.84	2.10	1.83	1.75	1.85	1.75
Square 90° gap	1.58	1.65	1.28	1.20	1.23	1.00
Simulation (90° gap)	1.80	2.10	1.86	1.69	1.85	1.75

inductances of these inductors were measured to be virtually unchanged from 20 Hz to 1 MHz, the results from Table III were used to estimate both the dc and ac magnetic fields during IBC operation of the inductors. For example, during direct coupling operation of the E-E core with 1 A injected into Y1 and G1 simultaneously, the dc flux at Y1 and G1 will be given by $\Phi(\mathrm{Y1})+\Phi(\mathrm{G1}) = 3.21\ \mu$Wb. Conversely, under the same conditions during inverse coupling operation, the total flux at Y1 and G1 will be $\Phi(\mathrm{Y1}) - \Phi(\mathrm{G1}) = 0.31\ \mu$Wb from data of Table III. Therefore, during IBC operation, the total magnetic fields resulting from the inductor current waveforms $(\mathrm{i}_1, \mathrm{i}_2)$, which are the combined ac and dc fields, are scale factors of the sum or differences defined above.

V. CONCLUSION

This paper describes and validates the developed analytical design relationships for interleaved boost converters using coupled inductors. Useful design equations for a magnetically coupled interleaved boost converter under continuous inductor current mode operation were summarized. Compared to the direct-coupling configuration, the inverse-coupling configuration provides the advantages of lower inductor ripple current and very low dc flux in the core. The direct-coupling configuration, on the other hand, provides the advantages of lower input ripple current and ac flux level. Therefore, the ac flux density-dependent core losses would be higher in an inverse-coupled converter whereas winding losses would be higher in a direct-coupled converter. Magnetic saturation due to dc flux is a greater design challenge with direct-coupled converters. Accordingly, an inverse-coupled configuration is the logical choice for high power interleaved boost converters. Empirical quantification of the predicted performance benefits of this power converter topology was presented via inductor simulation and converter performance data comparisons. It was shown that an inversely coupled interleaved power converter topology is superior for high power converter applications due to efficient dc flux cancellation characteristics as predicted. Three coupled inductor designs were investigated and compared within the 2-kW converter for average and peak flux considerations. Although all three inductors were oversized for the 2-kW converter power rating, the experiments and simulations enabled confident estimates of the performance of scaled coupled inductors with similar geometries. For example, the average magnetic field at Y2 for the square 45° core inductor while operating at $\mathrm{V_{in}} = 100$ V, $\mathrm{I_{in}} = 100$ A, in an inversely polarized IBC converter would be 417 G. With increasing emphasis in recent years on high power and high performance applications, the use of coupled inductor IBCs is seen to enable a potentially compact, high performance topology with very efficient core characteristics.

REFERENCES

[1] H. Kosai *et al.*, "Characterizing the effects of inductor coupling on the performance of an interleaved boost converter," in *Proc. CARTS USA 2009*, Mar. 2009, pp. 237–251.
[2] X. Huang *et al.*, "Parasitic ringing and design issues of digitally controlled high power interleaved boost converters," *IEEE Trans. Power Electron.*, vol. 19, no. 5, pp. 1341–1352, Sep. 2004.
[3] Y. Hu *et al.*, "Characteristics analysis of two-channel interleaved boost converter with integrated coupling inductors," in *Proc. IEEE Power Electronics Specialists Conf.*, Jun. 2006.
[4] Y. Hu *et al.*, "Design and implementation of two-channel interleaved boost converters with integrated coupling inductors," in *Proc. EPE-PEMC*, 2006, pp. 625–630.
[5] P. Thounthong *et al.*, "Design and implementation of 2-phase interleaved boost converter for fuel cell power source," in *Proc. IET Int. Conf. Power Electronics, Machines, and Drives*, Apr. 2008, pp. 91–95.
[6] W. Wen and Y. Lee, "A two-channel interleaved boost converter with reduced core loss and copper loss," in *Proc. IEEE Power Electronics Specialists Conf.*, Jun. 2004, pp. 1003–1009.
[7] P. Wong *et al.*, "Performance improvements of interleaving VRMs with coupling inductors," *IEEE Trans. Power Electron.*, vol. 16, no. 4, pp. 499–507, Jul. 2001.